Linking Snowpack Microphysics and Albedo Evolution

Mark G. Flanner and Charles S. Zender

Department of Earth System Science, University of California at Irvine

Abstract.

Snow aging causes reflectance to vary significantly on timescales of days. This variability influences the strength of snow-albedo feedback, and can affect the timing of snowmelt. However, climate models have yet to incorporate important controls on snow aging and albedo evolution. We develop a physically-based model that predicts evolution of dry, pure-snow specific surface area, and apply aspherical ice particle theory to link these results with albedo evolution. This is the first theoretical study to quantify the relative roles of initial size distribution, vertical temperature gradient, and snow density in snow albedo evolution. Vapor diffusion caused by curvature differences causes rapid albedo decay in the first day following snowfall. Vertical temperature gradient generally dominates grain growth processes afterward, but is modulated by snow density, irregularity in particle spacing, and temperature. These processes operate as a coupled system, which we uniquely represent without abrupt transitions between regimes.

Model results agree very well with measurements of isothermal snow evolution, and are within reasonable range of temperature gradient observations. We show that different snow state regimes cause albedo of non-melting snow surfaces with identical initial albedo to vary by 0.12 or more after 14 days. Lack of quality observational data illuminates the need for well-controlled snow studies that simultaneously monitor specific surface area, temperature gradient, and albedo. Accounting for snow aging processes, especially temperature gradient, will improve understanding and assessment of snow albedo feedback and climate sensitivity. The modeling framework we develop will also be useful for air-snow chemistry studies that consider specific surface area.

1. Introduction

The land surface plays an integral role in the planetary radiation budget. Snow is highly reflective and changes to its optical properties and spatial coverage modulate climate through snow-albedo feedback [e.g., *Budyko*, 1969; *Yang et al.*, 2001]. Slight changes in snow reflectance can double or halve the absorbed radiation, and many studies show snow to be a rapidly evolving medium [e.g., *McGuffie and Henderson-Sellers*, 1985; *Aoki et al.*, 2003; *Pirazzini*, 2004]. This evolution is an important consideration in global climate models (GCMs), where energy estimation errors due to poor radiative representation can affect the timing of snowmelt and then amplify biases through snow-albedo feedback [*Flanner and Zender*, 2005].

Previous studies account for the role of grain growth on albedo evolution only with empirical representations [e.g., *Verseghy*, 1991; *Marshall and Oglesby*, 1994; *Douville et al.*, 1995; *Loth and Graf*, 1998]. *Marshall* [1989] parameterizes snow albedo for use in climate models, including a description of the evolution of snow grain size in dry and melting snow. The parameterization describes a constant growth rate for the first two weeks after snowfall, based on limited grain-size measurements in polar, surface snow [*Stephenson*, 1967; *Warren et al.*, 1986]. Lack of observational data at the time prohibited her from deriving a temperature-dependence for grain growth during this initial growth phase. Using model results and recent observations, we will show that initial grain growth is non-linear and depends on snowpack temperature, initial size distribution, vertical temperature gradient (TG), and snow density.

Three recent studies demonstrate that representing ice media composed of non-spherical particles with a collection of spheres that conserves the total volume and total surface area (but not the total number of particles) yields predictions of hemispheric radiation fluxes typically within about 5% accuracy [*Grenfell and Warren*, 1999; *Neshyba et al.*, 2003; *Grenfell et al.*, 2005]. Suggested in earlier works [*Bryant and Latimer*, 1969; *Wiscombe and Warren*, 1980; *Pollack and Cuzzi*, 1980], this *equal-V/S* theory paves the way for an extremely powerful simplification that can be utilized when considering snow albedo evolution in GCMs, where generally only hemispheric fluxes are considered. It implies that if the specific surface area (SSA, $\hat{S}$, units of surface area per mass) of a snowpack is known, the snow can be represented optically with a collection of spheres, or effective radius (r_e), that conserves the snow's volume to surface area ratio, regardless of the snow's crystal habits. While this theory is of less use when directional reflectance is an important consideration [e.g., *Dozier*, 1989; *Painter and Dozier*, 2004], it can be utilized for estimation of the column energy budget in climate models. In support of this theory, we have found that snow reflectance predicted by different lognormal distributions of spheres which have the same volume to surface area ratio (but different mean radii, $\bar{r}$) are nearly identical over the entire solar spectrum.

Mean grain size of snowpacks generally increases with time, reducing albedo, especially in the near-infrared (near-IR) spectrum [e.g., *Wiscombe and Warren*, 1980]. Following snowfall and immediate mechanical deformation [*Jordan*, 1991], five primary processes govern the evolution of grain size. First, differences in curvature of the particles cause slight vapor density gradients via Kelvin's Law [e.g., *Colbeck*, 1980; *Arons and Colbeck*, 1995]. This process operates in isothermal snow, and can dominate grain growth on short timescales in fresh snow. Second, macroscopic TG in the snow causes sharp inter-granular vapor density gradients and bulk vapor diffusion through the ice matrix [e.g., *Marbouty*, 1980; *Colbeck*, 1983a; *Gubler*, 1985; *Sturm and Benson*, 1997], inducing *temperature gradient growth*. Third, snow subject to melting and refreezing experiences very dynamic growth as liquid H_2O is redistributed among the grains. Fourth, wind ventilation in surface snow also transports vapor. Finally, theory [*Zhang and Scneibel*,

0148-0227/06/$9.00

1995; *Colbeck*, 2001] and recent observations using scanning electron microscopy [*Rosenthal and Saleta*, 2006] indicate that sintering may be an important mechanism for reducing snow SSA in low TG environments. We treat the first two effects in this study. We will utilize empirical representations of wet snow metamorphism [*Brun*, 1989; *Marshall*, 1989] for future model development.

Snow albedo can also be strongly influenced by the accumulation of absorbing aerosols such as dust or soot [e.g., *Warren and Wiscombe*, 1980; *Hansen and Nazarenko*, 2004]. We neglect aerosols here, although the current study is a necessary precursor to understanding soot-albedo forcing because of the sensitivity of the forcing to snow grain size [*Warren and Wiscombe*, 1980]. In a coupled snow-aerosol model, aerosols will influence snow heating rates and affect grain growth through physically-realistic means.

The goal of this study is to apply basic microphysical principles to predict the evolution of dry snow SSA. Combined with *equal-V/S* theory, this will facilitate more realistic representation of snow albedo evolution. We prescribe snow temperature, temperature gradient, and density, which are all prognostic variables in many land surface models [e.g., *Oleson et al.*, 2004]. Thus, our microphysical module could be coupled to existing snow climate models [e.g., *Jordan*, 1991] without changing the bulk thermodynamics. Developing a full thermodynamic snow model is beyond the scope of this study. Our parameterization will be constrained by observation, and be suitable for snowpack studies across a range of spatial scales.

2. Theory and Methods

Vapor diffusion causes complex morphological changes to snow grains, forming intergranular bonds, faceted depth hoar crystals, and other complex shapes [e.g., *Sturm and Benson*, 1997]. Several studies have attempted to model dry snow metamorphism, accounting for some shape evolution in order to understand mechanical and thermal snow properties, with a motivation of understanding avalanche formation [*Gubler*, 1985; *Brown et al.*, 2001; *Lehning et al.*, 2002]. Because our goal is to predict evolution only of snow SSA and albedo, we adopt a more simplified approach to understanding grain growth, developing a one-dimensional representation of a collection of ice spheres.

Snow aging enhances our SNow, ICe, and Aerosol Radiative (SNICAR) model [*Flanner and Zender*, 2005], which represents radiative transfer in the snowpack. SNICAR is a multi-layer two-stream model based on *Wiscombe and Warren* [1980] and *Toon et al.* [1989] that treats snow as a collection of ice spheres. It obtains Mie parameters (single scattering albedo, extinction coefficient, and asymmetry parameter) for any lognormal size distribution from a lookup table computed offline. The model depends on vertically-resolved effective radius (r_e), solar zenith angle, snow depth and density, direct and diffuse incident radiation, bare surface reflectance, and concentrations of absorbing impurities. We use 470 radiative bands in the solar spectrum (0.3–5.0 μm). In this study, we assume direct and diffuse incident fluxes that are typical of mid-latitude winter.

2.1. Curvature Growth

We begin with general theory of diffusional growth of spherical ice particles. All symbols discussed here are listed in Appendix A. Fick's Law, in the absence of any convection, describes diffusion of vapor through air in the presence of a vapor density gradient, $\mathrm{d}\rho_\mathrm{v}/\mathrm{d}z$ as:

$$J_\mathrm{v} = -\mathrm{D}_\mathrm{v}\,\frac{\mathrm{d}\rho_\mathrm{v}}{\mathrm{d}z} \tag{1}$$

where D_v is the diffusivity of water vapor in air and is dependent on temperature [*Pruppacher and Klett*, 1998]. A convection term (simply wind vector multiplied by vapor density) is sometimes included in Equation 1, but we neglect it in this study because of large uncertainty about circulation processes within the snowpack. We note, however, that wind has competing effects on albedo evolution. High sublimation rates and delayed settling of the finest suspended crystals from wind-entrained snow leave a surface composed of small crystals [*Grenfell et al.*, 1994]. Conversely, wind accelerates grain growth by circulating vapor quickly through surface snow [*Cabanes et al.*, 2003].

Assuming an ambient vapor density, $\rho_{\mathrm{v,amb}}$ and vapor density $\rho_{\mathrm{v,s}}$ at the particle surface, the steady-state concentration profile at radial distance x, derived from the diffusion equation, is [e.g., *Seinfeld and Pandis*, 1998]:

$$\rho(x) = \rho_{\mathrm{v,amb}} - \frac{r}{x}(\rho_{\mathrm{v,amb}} - \rho_{\mathrm{v,s}}) \tag{2}$$

where r is the particle's radius. The mass growth rate of a particle is:

$$\frac{\mathrm{d}m}{\mathrm{d}t} = 4\pi r^2 \mathrm{D}_\mathrm{v} \left(\frac{\mathrm{d}\rho_\mathrm{v}}{\mathrm{d}x}\right)_{x=r} \tag{3}$$

Combining Equations 2 and 3, we get the general form of the steady-state growth equation for motionless aerosols employed in cloud and snow physics [e.g., *Colbeck*, 1983a; *Pruppacher and Klett*, 1998; *Seinfeld and Pandis*, 1998]:

$$\frac{\mathrm{d}m}{\mathrm{d}t} = 4\pi r \mathrm{D}_\mathrm{v}(\rho_{\mathrm{v,amb}} - \rho_{\mathrm{v,s}}) \tag{4}$$

The difference between ambient vapor density and vapor density at the particle surface drives growth or sublimation of the ice particle. In the continuum regime, $\rho_{\mathrm{v,s}}$ is assumed to be in constant equilibrium with the particle surface during growth because growth progresses hundreds of times more slowly than diffusion to the particle surface [*Seinfeld and Pandis*, 1998]. *Colbeck* [1983b] also discusses why surface kinetic effects are small. Thus, neglecting any solute effects, $\rho_{\mathrm{v,s}}$ is a function only of particle temperature and radius of curvature. For non-spherical ice shapes, the term $4\pi r$ may be replaced with an equivalent 'capacitance' for the shape, derived from electrostatic theory [e.g., *Pruppacher and Klett*, 1998], but these solutions are non-trivial [*Chiruta and Wang*, 2003].

Kelvin's Law demonstrates that equilibrium vapor pressure over curved surfaces exceeds that over planar surfaces [e.g., *Pruppacher and Klett*, 1998]:

$$p_\mathrm{s}(r,T) = p_\mathrm{eq} \exp\left(\frac{2\gamma}{\mathrm{R_v} T \rho_\mathrm{i} r}\right) \tag{5}$$

where p_eq is the saturation vapor pressure over a planar surface, γ the surface tension of ice against air, $\mathrm{R_v}$ the specific gas constant for vapor, T the system temperature, and ρ_i the density of ice. We use $\gamma = 0.109\,\mathrm{J\,m^{-2}}$ from *Pruppacher and Klett* [1998]. Corresponding vapor density can be easily found with the Ideal Gas Law. The surface saturation ratio ($p_\mathrm{s}/p_\mathrm{eq}$) is only about 1.021 and 1.002 for $r = 0.1\,\mu\mathrm{m}$ and $r = 1\,\mu\mathrm{m}$, respectively, and is very close to 1 for $r > 10\,\mu\mathrm{m}$. While such small grain sizes are atypical of snow, fresh snow typically has branch dendrites with sharp curvature. Thus the Kelvin Effect is an important consideration in fresh snow [*Colbeck*, 1980, 1983a], but otherwise does not contribute to significant vapor density gradients.

As sublimation or condensation occurs on a particle, latent heat is released or absorbed, altering the particle temperature. This temperature change has the effect of slowing both sublimation and condensation rates. An analytic approximation is derived for a particle's mass rate of change which accounts for the latent heat effect [e.g., *Rogers and Yau*, 1994; *Seinfeld and Pandis*, 1998]. We define it here in terms of the environmental vapor pressure p_{amb}:

$$\frac{\mathrm{d}m}{\mathrm{d}t} = \frac{4\pi r\,\frac{p_{amb} - p_\mathrm{s}(r,T)}{p_\mathrm{eq}}}{\left(\frac{\mathrm{L}}{\mathrm{R_v}T} - 1\right)\frac{\mathrm{L}}{\mathrm{K}T} + \frac{\mathrm{R_v}T}{p_\mathrm{eq}\mathrm{D_v}}} \tag{6}$$

where K is the temperature-dependent thermal conductivity of air [*Seinfeld and Pandis*, 1998], and L is the latent heat of sublimation. Relative to Equation 4, this approximation predicts differences in SSA of only about 4% after 14 days.

The key challenge, especially for TG conditions, is the determination of p_{amb}. We do not know of any measurements of relative humidity inside the snowpack. But air in surface snow is well-mixed with the lower atmosphere, and thus likely has a similar vapor density. Indeed, seasonal sublimation totaling 15% of snowfall is observed in the Colorado Front Range [*Hood et al.*, 1999]. During night, vapor saturation can induce frost deposition of small, ornate crystals, brightening the surface [*Pirazzini*, 2004]. In subsurface snow, we expect the interstitial pore space to be consistently near saturation, given the high density of solid surface. In a coupled snow-atmosphere model, p_{amb} could be predicted for surface snow from atmospheric conditions. But in this model we assume it is a volume-weighted mean of the equilibrium vapor pressures of all snow grains, as suggested by *Adams and Brown* [1982, 1983]:

$$p_{amb} = \int_0^\infty p_{\mathrm{s}}(r,T)\, r^3 P(r)\, \mathrm{d}r \tag{7}$$

where $P(r)$ is the probability density function of particles with radius r. As we will see later, this formulation also facilitates a consistent representation of TG growth.

For typical size distributions of snow grains, this weighted-mean predicts mean pore vapor pressure slightly greater than equilibrium with respect to planar ice. Thus, the smallest grains sublimate, while larger grains slowly grow. This formulation does not conserve mass (total ice mass only decreases with time, however), but as described earlier, the goal of this model is to predict SSA evolution using prescribed snow state variables. Furthermore, modeling the system as a closed-box is made difficult by the fact that ice mass is about five orders of magnitude greater than vapor mass for typical snow density and temperature. We found that preventing numerical oscillations in pore vapor pressure requires model timestep on the order of 10^{-4} s, starting from non-equilibrium conditions. In reality, however, sublimated vapor slightly raises local pore vapor pressure, inducing deposition on neighboring surfaces, including concave necks that bond sintered grains [*Miller*, 2002; *Miller et al.*, 2003]. Incorporation of geometry with negative radius of curvature would enhance the Kelvin Effect. But the geometry suggested by *Miller* [2002] predicts concave ice volume that is a very small fraction of total ice volume, and would hardly affect p_{amb} with our formulation.

We assume a lognormal distribution of grain radii with initial geometric standard deviation σ_{g} and number-median radius r_{n}:

$$n(r) = \frac{1}{\sqrt{2\pi}\, r\, \ln(\sigma_{\mathrm{g}})} \exp\left[-\frac{1}{2}\left(\frac{\ln(r/r_{\mathrm{n}})}{\ln(\sigma_{\mathrm{g}})}\right)^2\right] \tag{8}$$

where $n(r)$ is scaled to the probability density function $P(r)$. Our parameter of interest is $\hat{S}$, which is simply total surface area of the particle ensemble divided by total mass:

$$\hat{S} = \frac{3\int_0^\infty r^2 P(r)\,\mathrm{d}r}{\rho_{\mathrm{i}} \int_0^\infty r^3 P(r)\,\mathrm{d}r} \tag{9}$$

Similarly, effective radius, which drives the radiative transfer model, is also a surface area-weighted radius of the ensemble, and is directly related to $\hat{S}$ for any collection of particles as:

$$r_{\mathrm{e}} = \frac{3}{\rho_{\mathrm{i}}\, \hat{S}} \tag{10}$$

Finally, r_{n} is related to r_{e} for a lognormal distribution as:

$$r_{\mathrm{n}} = r_{\mathrm{e}} \exp\left[-\frac{5}{2}\ln(\sigma_{\mathrm{g}}^2)\right] \tag{11}$$

The initial size distribution determines the ensemble growth rate. Broad distributions with small median radii grow quickly as small particles completely sublimate, and monodisperse distributions do not evolve at all. Small size bins disappear permanently when all of their mass sublimates, and the distribution becomes non-lognormal. Assuming a broad distribution of r for fresh snow hopefully captures realistic range of surface curvatures.

2.2. Temperature Gradient Growth

Temperature gradient growth is a complex and poorly understood phenomenon. General observations of particle growth rates under TG are that they:

1. increase with increasing TG [*Marbouty*, 1980; *Fukuzawa and Akitaya*, 1993], probably up to some limiting value.

2. increase with increasing temperature [*Marbouty*, 1980], and have little dependence on TG at low temperatures [*Kamata et al.*, 1999]

3. increase with decreasing snow density [*Marbouty*, 1980; *Sokratov*, 2001; *Schneebeli and Sokratov*, 2004]

4. decrease with time and increasing particle size [*Sturm and Benson*, 1997; *Baunach et al.*, 2001]

Our approach captures these observations and represents curvature and TG growth in a unified manner. If we assume saturated pore vapor pressure along the temperature gradient axis, we can solve Equation 1 for $\mathrm{d}\rho_{\mathrm{v}}/\mathrm{d}z$ in terms of the temperature gradient $\mathrm{d}T/\mathrm{d}z$ to get the macroscopic vapor flux [*Baunach et al.*, 2001]:

$$J_{\mathrm{v}}\left(T, \frac{\mathrm{d}T}{\mathrm{d}z}\right) = -\mathrm{D}_{\mathrm{v}}\, \frac{p_{\mathrm{eq}}(T)}{\mathrm{R_v}T^2}\left[\frac{L}{\mathrm{R_v}T} - 1\right]\frac{\mathrm{d}T}{\mathrm{d}z} \tag{12}$$

$\mathrm{d}T/\mathrm{d}z$ is sign-dependent, but we always refer to it as positive in this study because of model symmetry along the TG axis. Conservation of mass requires that:

$$\frac{\mathrm{d}J_{\mathrm{v}}}{\mathrm{d}z} = -\frac{\mathrm{d}\rho_{\mathrm{v}}}{\mathrm{d}t} \tag{13}$$

Microphysical studies either assume $\mathrm{d}J_{\mathrm{v}}/\mathrm{d}z = \mathrm{d}\rho_{\mathrm{v}}/\mathrm{d}t = 0$ [e.g., *Adams and Brown*, 1983; *Gubler*, 1985], or just $\mathrm{d}\rho_{\mathrm{v}}/\mathrm{d}t = 0$ [*Baunach et al.*, 2001; *Lehning et al.*, 2002]. The latter studies predict a vertical flux divergence, but conserve mass by depositing all excess vapor, equaling $\mathrm{d}J_{\mathrm{v}}/\mathrm{d}z \times \Delta z$, as ice. With this assumption, the densification of snow ($\mathrm{d}\rho_{\mathrm{s}}/\mathrm{d}t$) equals the divergence in vertical flux, and is proportional to both $\mathrm{d}^2T/\mathrm{d}z^2$ and $(\mathrm{d}T/\mathrm{d}z)^2$ [*Giddings and LaChapelle*, 1962]. This approach was used by *Sturm and Benson* [1997] to calculate relative minima and maxima density positions in sub-Arctic snowpack, assuming measured temperature profiles.

Applying this theory to grain growth, however, by distributing the excess vapor to available grains in any reasonable way, underpredicts grain growth by 1–2 orders of magnitude. Deficiency in this macroscopic approach suggests that vapor flux must occur on very small (i.e., inter-particle) spatial scales. Evidence for this comes from measurements indicating that water molecules composing individual grains must sublimate and re-deposit many times over during the course of a winter [*Sturm and Benson*, 1997]. Presumably, this deficiency is also why *Baunach et al.* [2001] and *Lehning et al.* [2002] add an intra-lattice vapor flux to their vertical flux divergence term in the Swiss SNOWPACK model. Realizing that interparticle vapor flux is required to achieve observed growth rates, early modeling studies have considered coupled source-sink particle configurations analogous to electrostatic capacitors [*Colbeck*, 1983a, b; *Sommerfeld*, 1983; *Gubler*, 1985; *Colbeck*, 1993].

Because ice conducts heat about 100 times more efficiently than air [*Giddings and LaChapelle*, 1962], we expect temperature gradient to be enhanced across the pore, relative to the macroscopic gradient. Therefore, the top of a grain will tend to be warmer than its environment, and the bottom colder, causing growth from

the bottom and sublimation from the top. Observations of grains with rounded tops and faceted bottoms support this theory [*Colbeck*, 1983a; *Sturm and Benson*, 1997]. But if we consider regular spacing between grains in a uniform vapor gradient field, all grains should have almost zero net growth resulting from TG (the only growth resulting from the slow, bulk vapor flux, Eq. 12). The importance of irregular spacing for particle growth has been recognized [*Colbeck*, 1983a; *Sommerfeld*, 1983; *Gubler*, 1985]. Observations that only about 1 in 10 grains survive a season in a large temperature gradient [*Sturm and Benson*, 1997] offer strong evidence of preferential growth sites and competition for vapor. Observations of the largest crystals being surrounded by greater pore volumes [*Akitaya*, 1974; *Colbeck*, 1983a] imply greater vapor source for these particles and offer further evidence for the importance of particle spacing. Presumably, this is also why lower density snow experiences more rapid growth [*Marbouty*, 1980; *Fukuzawa and Akitaya*, 1993]. Realizing the importance of irregularly-spaced particles for growth, it is not surprising that growth occurs faster in greater temperature gradients [*Marbouty*, 1980; *Fukuzawa and Akitaya*, 1993], as enhanced vapor density gradients accentuate minute advantages in grain positioning. These realizations helped motivate the early capacitor models, but they have the burden of manually designating source and sink particles.

In reality, the net growth or decay experienced by a particle depends on the sum contributions from all pore vapor sources/sinks. Our model assumes a single pore source/sink for each particle which accounts for all sources and sinks. To achieve this, we assign a single particle-pore distance vector, $\vec{h}$, to each particle, representing the vector sum of all particle-pore distances along the TG axis. Neglecting the Kelvin Effect, the sign of $\vec{h}$ determines growth or sublimation, and the magnitude determines mass rate of change, as greater spacings imply greater vapor pressure differences. In a regular-packed lattice, $\vec{h}$ would be zero for every particle because each particle would have equally-strengthed sources and sinks (again neglecting the small bulk flux from Equation 12), and only curvature growth would occur. To account for heterogeneous particle positioning, we synthesize Gaussian distributions of $\vec{h}$ for each particle size, with means equal to zero.

But what is the standard deviation of $\vec{h}$? It is directly related to interparticle spacing variability, but lacking observations of such, we define a tunable parameter, ϕ, representing the degree of irregularity in particle packing, to scale the standard deviation of $\vec{h}$ to the mean particle spacing, $\bar{a}$. The mean spacing between particle boundaries depends on snow density (ρ_s) and particle size as:

$$\bar{a}(r, \rho_\mathrm{s}) = \left(\frac{4\pi r^3 \rho_\mathrm{i}}{3\rho_\mathrm{s}} \right)^{1/3} - 2r \tag{14}$$

These ideas conform with [*Colbeck*, 1993], who considers distributions of the normalized quantity $(a + 2r)/r - 2$. If we assume the same distribution of this quantity applies to all particle sizes, then mean spacing and standard deviation are related by the same scaler quantity for every particle size. With these arguments, we define a Gaussian probability density function of $\vec{h}$, given particle size and snow density, $P(\vec{h} \,|\, r, \rho_\mathrm{s})$, which has zero mean and standard deviation $\phi\,\bar{a}$. We can see that $\bar{a} \to 0$ as $\rho_\mathrm{s}/\rho_\mathrm{i} \to \pi/6$. Therefore, TG growth ceases at the limit $\rho_\mathrm{s} = 480\,\mathrm{kg\,m^{-3}}$. Snow densities this high are rare in seasonal snowpack. Our limit is greater than the observed limit of $350\,\mathrm{kg\,m^{-3}}$ for TG growth forms [*Marbouty*, 1980], but our model predicts very slow growth at high densities.

Having defined a representative particle-pore parameter $\vec{h}$, we assume the pore vapor density is the mean of the equilibrium vapor densities at the top and bottom of the pore [*Adams and Brown*, 1982, 1983; *Colbeck*, 1983b]. This stems from the assumption that, on small spatial scales, $\mathrm{d}J_\mathrm{v}/\mathrm{d}z = 0$, and therefore, neglecting minuscule change in $\mathrm{D_v}$, $\mathrm{d}^2\rho_\mathrm{v}/\mathrm{d}z^2 = 0$ (Equations 1 and 13). Considering non-zero values of these terms, however, would alter our growth rates very little, as described above. Maintaining consistency with our curvature model, the equilibrium vapor densities at either pore boundary are also volume-weighted means of the ensemble of particle equilibrium vapor densities [*Adams and Brown*, 1982, 1983]. Then, the ambient pore vapor pressure, respective to each particle size and particle-pore spacing, is:

$$p_{amb}(r, \vec{h}) = \frac{1}{2}\left(T - \vec{h}\,\frac{\mathrm{d}T}{\mathrm{d}z}\right)\left[\frac{\int_0^\infty p_\mathrm{s}(r,T) r^3 P(r)\,\mathrm{d}r}{T} + \frac{\int_0^\infty p_\mathrm{s}\left(r, T - 2\vec{h}\,\frac{\mathrm{d}T}{\mathrm{d}z}\right) r^3 P(r)\,\mathrm{d}r}{T - 2\vec{h}\,\frac{\mathrm{d}T}{\mathrm{d}z}}\right] \tag{15}$$

Note that $\vec{h}$ designates vertical distance from pore center to particle center (rather than particle boundary) to account for the enhanced TG across the pore [*Colbeck*, 1983a], discussed above. Particle centers and pores at the same vertical level ($\vec{h} = 0$) are at the same temperature, and no vapor diffuses between them. With a TG of zero, Equation 15 reduces exactly to Equation 7, irrespective of grain size. Thus, we have a unified expression for ambient vapor pressure that includes the Kelvin Effect and TG effects. With p_{amb} determined, Equation 6 drives the growth or sublimation of all particles. While the mean particle-pore spacing is zero for all particle sizes, appreciable growth of the ensemble occurs because the sublimating particles disappear completely, leaving behind only growing ones. In the studies described below, we use a timestep of 3600 s, 200 size bins, and 40 spacing bins per size bin.

3. Results and Discussion

In this section we compare predictions by SNICAR with observations of isothermal snow SSA evolution and grain size evolution in snow with temperature gradient. Then, we show dependence of snow albedo evolution on snow properties, and compare SNICAR albedo with one 10-day observational timeseries. Finally, we discuss a simple and effective parameterization of SSA evolution suitable for climate models and air-snow chemistry studies [e.g., *Domine and Shepson*, 2002].

3.1. Isothermal SSA Evolution

We first compare model predictions of isothermal growth with recent controlled laboratory experiments from *Legagneux et al.* [2004]. They gathered snow as it was falling and stored it at liquid nitrogen temperatures to prevent grain growth before measurement. During the experiment, they kept the snow uniformly at $-15\,^\circ\mathrm{C}$, and observed SSA evolution by measuring methane adsorption. They provide a physical basis for representing time-dependent SSA with an equation of the form:

$$\hat{S}(t) = \hat{S}_0 \left(\frac{\tau}{t + \tau}\right)^{(1/\kappa)} \tag{16}$$

where $\hat{S}_0$ is the initial SSA, and τ and κ are empirical parameters. As we show later, this function also robustly fits model predictions over a range of temperature, TG, and density.

We compare measurement and model results using different initial size distribution widths (σ_g). *Legagneux et al.* [2004] provide best-fit parameters of Equation 16 for their measurements, which we reproduce in Table 1. We set $\hat{S}_0$ and T to match the snow samples. Figure 1 shows model results against observation for their three fresh snow samples. SNICAR reproduces observed SSA decay from samples 1 and 2 quite well using $\sigma_\mathrm{g} = 2.3$, but struggles to capture the long-term decay manifested in sample 3. Our

Table 1. Parameters $\hat{S}_0$, κ, and τ for observations of fresh snow evolution from Table III of *Legagneux et al.* [2004]

Sample	$\hat{S}_0(\mathrm{m^2\,kg^{-1}})$	τ(hours)	κ
1	87	7.1	4.6
2	100.7	10.2	3.6
3	59.2	12.5	4.1

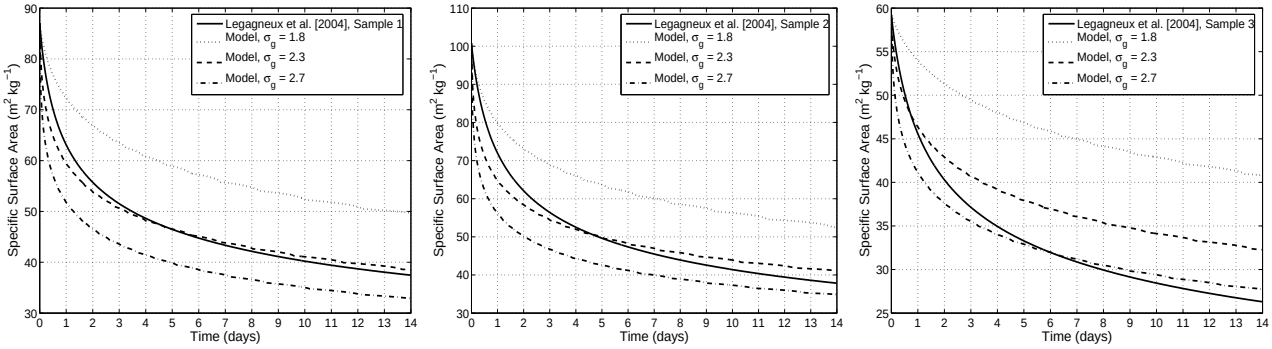

Figure 1. Comparison of model predictions of isothermal specific surface area evolution with measurements from *Legagneux et al.* [2004]. The three panels each show one observed timeseries and three modeled timeseries, assuming different initial size distribution widths. Model initial effective radius is chosen to match initial observed SSA.

choices of $\sigma_{\rm g}$ are within reasonable range of observed $\sigma_{\rm g}$. Using data provided by Teruo Aoki, we fit lognormal distributions to measurements of thousands of snow grains from four different snow samples [*Aoki et al.*, 2000]. The best-fit values of $\sigma_{\rm g}$ for the four collections are 1.75, 1.80, 1.78, and 2.20. The snow studied by *Aoki et al.* [2000] was at least a day old, however, and we expect the size distribution to narrow with time, as small grains disappear. We also expect real variability in $\sigma_{\rm g}$ for fresh snow. Furthermore, we are likely accounting for the greater range of *curvatures* in real, aspherical grains by assuming a broader distribution of spherical grains. The robustness of modeling SSA evolution with spheres must be tested against observations under variable snow temperatures though.

Conditions which favor rapid curvature growth are wide size distributions of small particles. In Figure 1, SSA decreases rapidly during the initial day or two following snowfall, and subsequently tapers off as the distribution narrows and mass becomes concentrated with larger grains. Grain growth in the first two days has a strong dependence on $\sigma_{\rm g}$, while growth after about day 3 has little dependence on $\sigma_{\rm g}$. These model results are also supported by observations of temporal decrease in grain curvature of fresh snow [*Fierz and Baunach*, 2000].

3.2. Temperature Gradient Evolution

Snow can be subject to TG well in excess of $100\,{\rm K\,m^{-1}}$ [*Fukuzawa and Akitaya*, 1993; *Sturm and Benson*, 1997]. Cold, clear-sky nights favor large gradients, as strong radiative emission cools the snow surface more than the lower atmosphere, while snow at depth can remain near the melting temperature. With a goal of understanding avalanche formation, several studies have measured grain growth of high density, large-grained snow (characteristic of basal snow) subject to large TG over long time-periods [*Marbouty*, 1980; *Sturm and Benson*, 1997; *Baunach et al.*, 2001; *Lehning et al.*, 2002]. These conditions induce depth-hoar formation, which is mechanically weak. *Fukuzawa and Akitaya* [1993], however, show that depth hoar can form very rapidly in surface snow.

We compare model predictions with *Fukuzawa and Akitaya* [1993]. In laboratory studies, they induced temperature gradients from 150 to 300 $\rm K\,m^{-1}$ in low density snow (80–100 $\rm kg\,m^{-3}$) made with an ice-slicer. They maintained a mean temperature of $-16\,^{\circ}{\rm C}$ at the sampling depth (1 cm). They report mean diameter, $\bar{d}$, as that of spheres with equal cross-sectional area as the photographed crystals, and note that this method can lead to high estimation biases. Experiments were conducted for up to 50 hours. We replicated these experimental conditions for all temperature gradients with SNICAR, using different values of ϕ, and present a scatterplot of modeled *vs.* observed mean radius in Figure 2.

Fukuzawa and Akitaya [1993] observe highly linear growth rates, whereas SNICAR predicts more rapid initial growth that tapers off. Based on our isothermal snow analysis, we used $\sigma_{\rm g} = 2.3$, while snow produced by an ice-slicer may be more homogeneously-sized. However, we do not attribute the non-linear growth evolution to curvature effects, as a sensitivity study with monodisperse grain size showed only slightly more linear growth. The large TG of these studies overshadows any curvature effects, except in the first couple of hours. Interestingly, similar non-linear growth functions have been observed in long-term, high TG studies [*Sturm and Benson*, 1997; *Baunach et al.*, 2001], as mentioned above. Nonetheless, model-measurement agreement is quite good when we assume $\phi = 5$. Also, while we must use mean radius, $\bar{r}$ for comparison with *Fukuzawa and Akitaya* [1993], we emphasize that it is not the parameter of interest, having little bearing on snow radiative properties. In fact, the time-progression of $\bar{r}$ and $r_{\rm e}$ can be *inversely* related if mass transfer is skewed towards one end of a broad size distribution. Hence, model-measurement agreement of $\bar{r}$ is no guarantee that SNICAR predicts realistic albedo evolution. *Fukuzawa and Akitaya* [1993] is, however, the most relevant and comprehensive observational study on TG growth that we are aware of.

Table 2. Long Term Temperature Gradient Growth

Time	Mean Radius (μm)			
	Observation	Mdl($\phi = 3$)	Mdl($\phi = 5$)	Mdl($\phi = 7$)
[*Baunach et al.*, 2001], $\mathrm{d}T/\mathrm{d}z = 30$, $\rho_{\rm s} = 200$, $T = 269$				
0 days	135	135	135	135
23 days	415	318	387	444
30 days	455	355	435	501
[*Lehning et al.*, 2002], $\mathrm{d}T/\mathrm{d}z = 240$, $\rho_{\rm s} = 120$, $T = 263$				
0 days	261	261	261	261
12.7 days	1345	895	1135	1338
[*Lehning et al.*, 2002], $\mathrm{d}T/\mathrm{d}z = 160$, $\rho_{\rm s} = 140$, $T = 263$				
0 days	256	256	256	256
12.9 days	1174	702	877	1024
[*Lehning et al.*, 2002], $\mathrm{d}T/\mathrm{d}z = 35$, $\rho_{\rm s} = 210$, $T = 263$				
0 days	256	256	256	256
30 days	713	457	548	625

We also compare model predictions with two long-term laboratory observations, presented in Table 2. These studies examine growth in denser, larger-grained snow. They have less relevance to surface snow, but nonetheless offer some insight into SNICAR's performance. *Baunach et al.* [2001] use the same equal-area method for determining grain size as *Fukuzawa and Akitaya* [1993] and *Lehning et al.* [2002] publish grain size referring to the

Table 3. Experimental Configurations for Figure 3

	Exp. A	Exp. B	Exp. C	Exp. D
$\sigma_{\rm g}$	$1.25 - 3.5$	2.3	2.3	2.3
$r_{\rm e0}$ [μm]	50, 100	50	50	50
Initial Alb.	0.854, 0.825	0.854	0.854	0.854
$T\,[^{\circ}{\rm C}]$	-5	$-50 - 0$	-5	-5
$\mathrm{d}T/\mathrm{d}z\,[{\rm K\,m^{-1}}]$	0	20	$0 - 250$	100
$\rho_{\rm s}\,[{\rm kg\,m^{-3}}]$	N/A	100	100	$50 - 480$

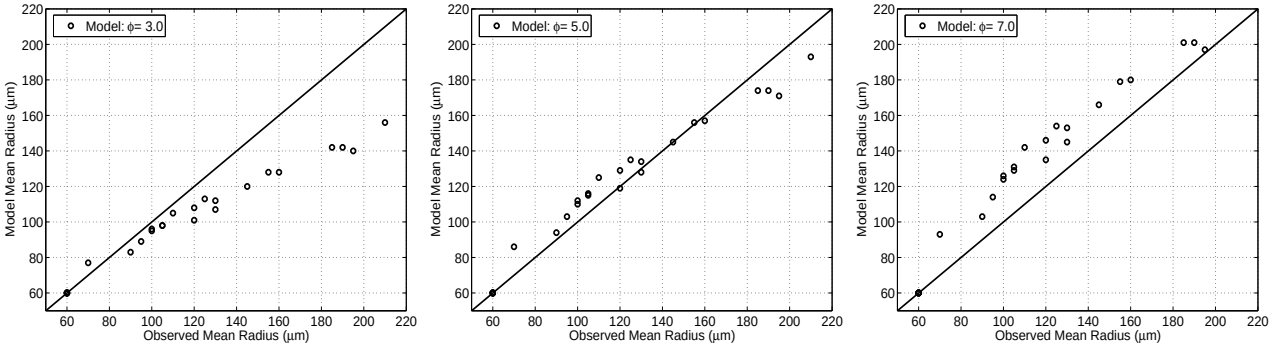

Figure 2. Comparison of model-predicted mean radius with observations from *Fukuzawa and Akitaya* [1993] under temperature gradients of 150, 200, 250, and 300 K m^{-1}. The three panels illustrate the affect of increasing standard deviation of inter-particle spacing (left to right), defined by model parameter ϕ.

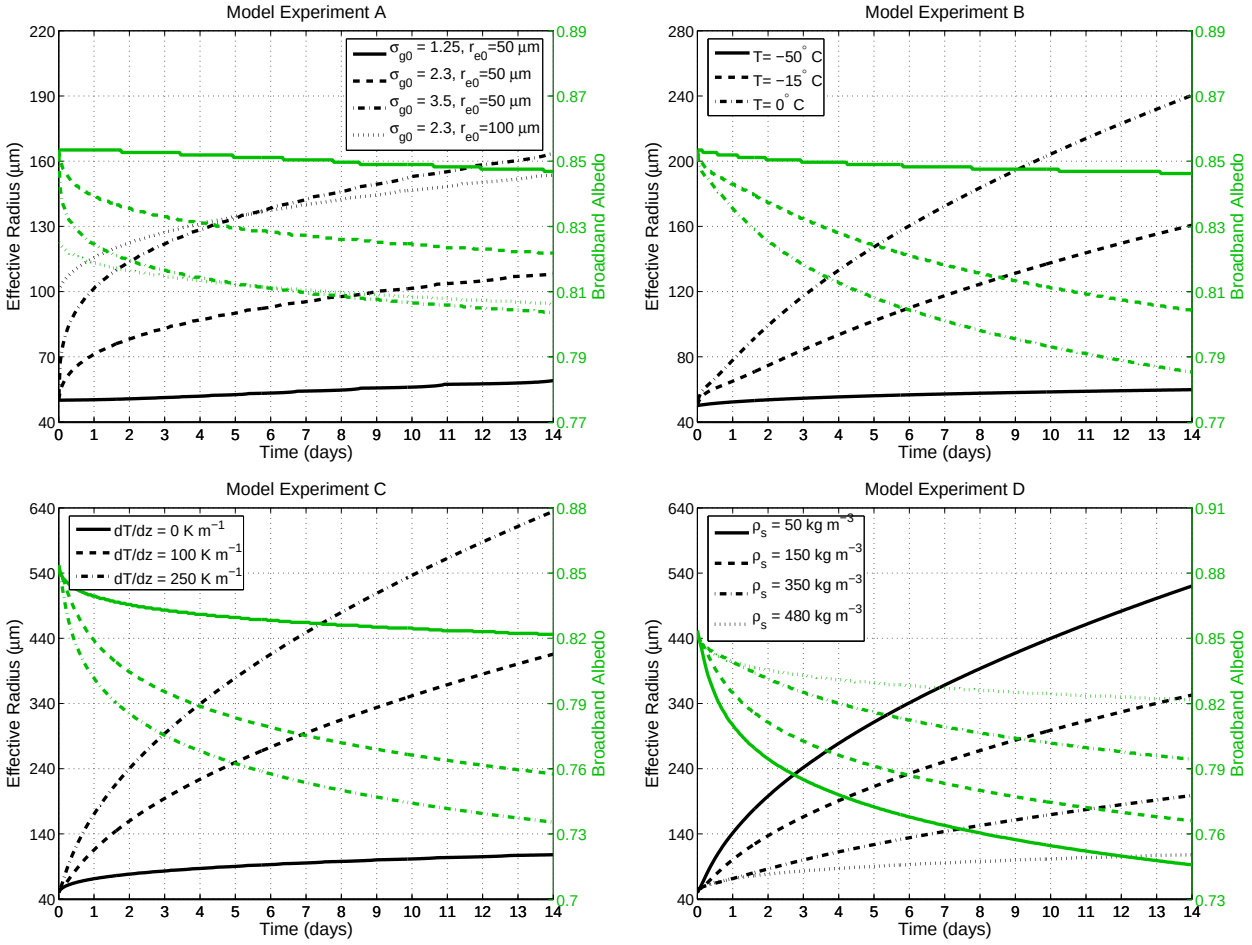

Figure 3. Model parameter study illustrating the evolution of snow effective radius (r_e) and albedo evolution, isolating dependence of (top-left) initial size distribution, (top-right) temperature, (bottom-left) temperature gradient, and (bottom-right) snow density. Time evolution of effective radius is plotted in black against the left axis and broadband albedo in red against the right axis.

greatest extension of the grain. In the long-term, $\phi = 7$ provides better agreement with these data, but the measurement technique of *Lehning et al.* [2002] gives greater radius that the mean radius that we model.

Finally, we compared SNICAR predictions with recent observations of SSA evolution under TG conditions [*Schneebeli and Sokratov*, 2004]. They use X-ray computed microtomography (XMT) to observe 3-D snow microstructure undergoing TG metamorphism. While this technique holds excellent promise for understanding the physics of crystal metamorphism, as sublimation and deposition on individual crystals are observed real-time, SSA evolution was not the focus of this study. Unfortunately, SSA deduced from XMT depends on scan resolution, so results from this method are inconsistent with the gas adsorption technique [*Legagneux et al.*, 2004]. We found best agreement with their results using $3 < \phi < 5$, but hesitate to place much emphasis on XMT observations until they can be corroborated with gas adsorption results.

More controlled experiments of fresh snow SSA evolution are needed to realistically assess SNICAR's predictions of TG growth in the context of albedo evolution. Placing the heaviest emphasis on *Fukuzawa and Akitaya* [1993], and considering a mean value of the other studies, $\phi = 5$ is a reasonable assumption. We assume this value for the rest of the study, but should re-assess it as future observations becomes available.

3.3. Snow Albedo Evolution: Model Sensitivity to Physical Parameters

In this section we use SNICAR to examine the influence of σ_g, temperature, TG, and snow density on snow albedo evolution. Isolating these parameters also helps us assess if SNICAR captures the basic observations of TG growth listed in methods. Although r_e is most influential on near-IR albedo (0.7–5.0 µm), we only examine broadband albedo (0.3–5.0 µm). Grain size varies with snow depth, influencing bulk snow albedo [e.g., *Grenfell et al.*, 1994], but here we assume an optically-thick snowpack of uniform time-evolving effective grain size. SNICAR predicts broadband albedo variation of only 0.0075 when r_e varies from 50–500 µm beneath a 5 mm LWE layer with $r_e = 50$ µm. Thus, assuming a homogeneous, optically-thick snowpack is reasonable for fresh snowfall on top of existing snow. However, we expect r_e time-evolution to vary within a fresh snow layer in a strong surface TG. We assume direct incident flux with a zenith angle of 60 °. Model snowpack configurations for our four experiments are summarized in Table 3. Also listed are the initial snow albedos, corresponding to initial effective radii, r_{e0}. Equation 10 relates $\hat{S}$ to r_e, but we use r_e in these discussions because of its common use by the radiative transfer community.

Figure 3 shows the temporal evolution of r_e and albedo (plotted on different axes) for these configurations. Model Experiment A depicts isothermal snow evolution with four different initial size distributions. We see that large σ_g drives rapid initial albedo decay. But comparison of the two $\sigma_g = 2.3$ simulations shows that larger initial effective radii mitigate the effect that large σ_g can have by reducing the Kelvin Effect. Only the combination of small r_{e0} and large σ_g drives rapid initial albedo decay. After 14 days, however, the albedo range is only 0.04 for the given range of initial conditions.

Model Experiment B demonstrates the effect of temperature on albedo evolution while holding σ_g and r_{e0} fixed with a modest (also fixed) TG. In contrast to the effects of σ_g and r_{e0}, temperature differences produce widespread albedo differences with time. For this configuration and these three temperatures, the albedos after 14 days are 0.79, 0.81, and 0.85.

Model Experiment C isolates the influence of TG with all other initial parameters fixed. We see that, given realistic ranges of the physical parameters, TG can be the most influential on albedo. For this range of TG, albedo and r_e range by 0.09 and 530 µm, respectively, after 14 days. In a sensitivity test with $T = -50$ °C, albedo varied by only 0.017 after 14 days under the same range of TG. Thus, our model conforms with observation that TG becomes unimportant in colder snow [*Kamata et al.*, 1999]. We attribute this behavior to the non-linear dependence of saturation vapor pressure on temperature. Vertical vapor density gradients drive TG growth, and $\mathrm{d}\rho_v/\mathrm{d}z$ decreases with decreasing temperature in near-saturation conditions because of the Clausius-Clapeyron relationship.

Finally, model Experiment D shows that snow density also modulates the importance of TG. All albedo change with $\rho_s = 480\,\mathrm{kg\,m^{-3}}$ is from curvature growth, since $\bar{a} = 0$ (Equation 14). The range of albedo after 14 days for $50 < \rho_s < 350\,\mathrm{kg\,m^{-3}}$ is about 0.05. While *Marbouty* [1980] suggests that variable snow densities less than $150\,\mathrm{kg\,m^{-3}}$ do not affect TG growth, SNICAR predicts continual increasing influence as $\rho_s \to 0$. It may be reasonable to cap the effect of ρ_s at some low value, but given observational uncertainties and realistic snow densities, we refrain from doing so here.

3.4. Observed Albedo Evolution

At this time we cannot conduct a meaningful comparison of model and observed albedo evolution because:

1. We know of no observational studies simultaneously measuring albedo, temperature gradient, and size distribution.

2. Magnitudes of the competing wind effects (ventilation and fine crystal deposition) are unknown and not included in SNICAR.

3. We do not know the importance of, or consider, nighttime frost formation of fine, 'bright' crystals [e.g., *Pirazzini*, 2004].

4. Concurrent observations of albedo and accumulation of absorbing impurities, such as soot, are rare.

The paucity of data stresses the need for controlled studies which simultaneously measure albedo, vertically-resolved temperature, SSA, ρ_s, and accumulation of impurities at high temporal resolution, so the methods we discuss here can be better applied. In spite of these uncertainties, we include one timeseries of observed dry snow albedo evolution. Comparison of model predictions with these data demonstrates that SNICAR is capable of reproducing reality, whether for right or wrong reasons. More definitive conclusions about model performance can only be drawn when more comprehensive observational data becomes available.

We examined six years of data from the Subnivean site of the Niwot Ridge Long Term Ecological Research (LTER) site in Colorado [*Williams*, 2005], and five years of data from the Atmospheric Radiation Measurement (ARM) site at Barrow, Alaska. We isolated only one timeseries longer than five days, following a fresh snowfall event, in which there were consistent clear-sky or cloudy conditions, daily maximum temperature didn't exceed 0.5 °C, and there was no, or little, fresh snowfall.

The Jan. 2, 2001 Niwot Ridge snowfall event (81 mm LWE) was followed by 10 clear-sky days. Unfortunately, the temperature exceeded 0 °C (by only 0.5 °C) for three hours on the third day following snowfall, and a light snowfall of 2 mm LWE was also reported on this day. There is a very slight albedo increase this day, which likely tracks the snowfall, but could also be other variability. It is possible that the two effects partially canceled each other, or that they were both insignificant.

Figure 4 depicts the albedo evolution following this event, as measured at different times of the day, and also as predicted by SNICAR with different configurations. The data are hourly averages from 10-minute observations, and timeseries measured at the same time-of-day ensure nearly consistent zenith-angle. We also include snow aging parameterization from the NCAR Community Land Model 3 (CLM) [*Oleson et al.*, 2004], and NASA GISS GCM ModelE [*Schmidt et al.*, 2006], which is based on *Loth*

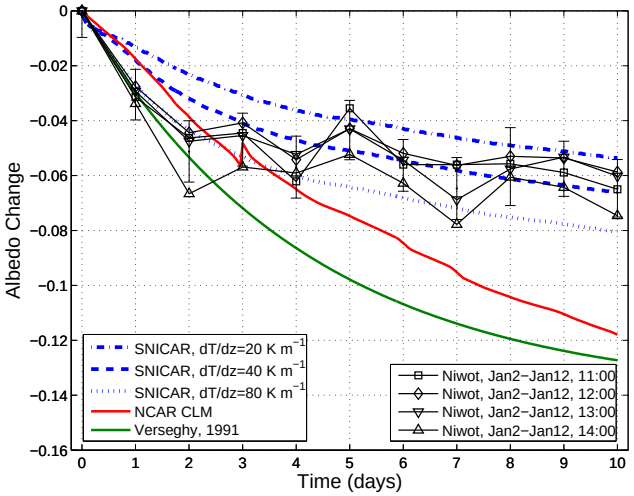

Figure 4. Observed and modeled albedo decay at Niwot Ridge following the January 2, 2001 snowfall event. Error bars represent one standard deviation of all measurements composing each day's albedo change.

and Graf [1998], who, in turn, uses albedo decay from *Verseghy* [1991] for dry, deep snow. CLM dry snow aging depends on snow temperature, while the non-melting relationships described by *Verseghy* [1991] and *Loth and Graf* [1998] do not. We have included the albedo increase that CLM would prescribe for the 2 mm LWE snowfall on day 3. To reduce zenith-angle dependence, all curves depict albedo change, rather than absolute albedo. The error bars represent one standard deviation of measured albedo reduction, centered about each day's mean albedo change. The 10-minute measurements are normalized to their base albedo at time zero, and the standard deviation is derived from all 24 daily measurements. The three SNICAR predictions are of direct-radiation albedo evolution with $\mathrm{d}T/\mathrm{d}z = 20$, 40, and $80\,\mathrm{K\,m^{-1}}$, assuming $\sigma_\mathrm{g} = 2.3$, $\rho_\mathrm{s} = 100\,\mathrm{kg\,m^{-3}}$, and vertically-homogeneous grain size ($r_\mathrm{e0} = 50\,\mu\mathrm{m}$), which is justified in this case because the snowfall event was large and rapid. SNICAR and CLM models are both driven with hourly mean air temperature, which we use as a rough surrogate for snow temperature. This assumption should cause little error for these conditions, as driving SNICAR with the mean (constant) temperature alters 10-day albedo change by $\sim 1\,\%$.

We make several observations here. First, the large 1-day albedo change (-0.03) is characteristic of rapid curvature growth. We can replicate this with small TG and $\sigma_\mathrm{g} > 2.3$, or with large TG. Second, $\mathrm{d}T/\mathrm{d}z = 80\,\mathrm{K\,m^{-1}}$ reproduces observed albedo decay during the first 4 days very well. Third, there is an albedo rise on Day 5 that could be explained by atmospheric- or frost- deposition of fine crystals, or noise. If deposition is the cause, grain growth of the underlying snow may proceed at a similar rate as predicted with $\mathrm{d}T/\mathrm{d}z = 80\,\mathrm{K\,m^{-1}}$. Fourth, SNICAR captures this observational trend better than the GCM parameterizations, which predict excessive albedo decay after day 3. CLM implicitly accounts for globally uniform accumulation of impurities, which is one reason for its greater predicted albedo reduction. In future GCM studies, we will account for time-dependent accumulation of impurities with on-line atmospheric transport and deposition.

3.5. Empirical Parameterization

Legagneux et al. [2004] propose Equation 16 as an empirical representation for observed isothermal SSA evolution. We show that Equation 16 robustly fits predictions of SSA evolution over a wide range of temperature, TG, and snow density. The simplicity of this equation is attractive because of the numerous size bins that SNICAR requires to capture curvature growth. Resulting computational savings open the door for its use in climate models and snow chemistry studies which utilize SSA.

We compute best-fit parameters τ and κ for Equation 16 to match 14-day simulated SSA over the domain $210 \le T \le 273\,\mathrm{K}$, $0 \le \frac{\mathrm{d}T}{\mathrm{d}z} \le 300\,\mathrm{K\,m^{-1}}$, and $50 \le \rho_\mathrm{s} \le 400\,\mathrm{kg\,m^{-3}}$. Figure 5 depicts time evolution of SSA predicted by SNICAR and Equation 16 with best-fit parameters over some of this domain. Agreement is exceptionally good, even with large TG and range of ρ_s. Best-fit parameters for the curves shown in this figure are listed in Table 4. Implementation of this method simply requires the time-derivative of Equation 16 and an online lookup table retrieving best-fit parameters as a function of T, $\mathrm{d}T/\mathrm{d}z$, and ρ_s. The authors can be contacted for a comprehensive table.

Table 4. Best-fit parameters of Equation 16 for the range of temperatures, temperature gradient, and snow density shown in Figure 5

			Snow Temperature (°C)			
$\mathrm{d}T/\mathrm{d}z$ ($\mathrm{K\,m^{-1}}$)	ρ_s ($\mathrm{kg\,m^{-3}}$)		−50	−20	−10	0
0	150	τ	43.6	7.1	4.5	3.2
		κ	11.4	6.7	6.1	5.8
50	150	τ	27.5	47.1	21.0	11.9
		κ	15.3	1.7	1.8	1.9
200	50	τ	370.6	5.2	2.5	1.5
		κ	0.9	1.9	1.9	1.9
200	300	τ	47.2	35.0	15.5	8.8
		κ	11.7	1.8	1.9	1.9

4. Conclusions

We have developed a new, physically-based model which predicts the evolution of dry snow specific surface area (SSA), and is suitable for coupling to full snow thermodynamic and air-snow chemistry models. Recent studies [*Grenfell and Warren*, 1999; *Neshyba et al.*, 2003; *Grenfell et al.*, 2005] justify use of snow SSA to obtain accurate hemispheric radiative fluxes, even for aspherical particles, thus linking our results to albedo evolution. Our model suggests that curvature-driven vapor diffusion dominates mass transfer of fresh snow under low temperature gradient. Vertical temperature gradients exceeding $20\,\mathrm{K\,m^{-1}}$, however, induce vapor density gradients which otherwise dominate grain growth and albedo decay. The influence of temperature gradient is controlled by temperature, snow density, and variance of interparticle spacing.

Model results track laboratory observations of isothermal SSA evolution very well. Predictions of temperature gradient growth compare favorably with observed mean radius evolution, but simultaneous measurements of SSA and temperature gradient are needed for thorough model evaluation. 14-day albedo change of dry snow with identical initial effective radii varies from -0.01 to -0.13, depending on snow conditions. Model predictions track one 10-day timeseries of clear-sky albedo measurements from Niwot Ridge better than two GCM parameterizations, but too little is known about the snowpack conditions to draw any definitive conclusions. Lastly, we show that a simple representation of SSA evolution robustly describes our model over a wide range of parameters. Its simplicity and effectiveness suggest that it could be a valuable addition to climate and snow chemistry models.

Existing GCM representations of snow aging do not consider temperature gradient in albedo evolution, although this and several other studies [*Marbouty*, 1980; *Fukuzawa and Akitaya*, 1993; *Sturm and Benson*, 1997] show it to be very important. Investigations into the effects of blowing snow, wind ventilation, and

Table 5. Appendix A: List of Symbols

Symbol	Description	Units
a	Particle boundary-boundary spacing	m
$\bar{a}$	Mean particle boundary-boundary spacing	m
$\mathrm{D_v}$	Diffusivity of vapor in air	$\mathrm{m^2\,s^{-1}}$
$\bar{d}$	Mean particle diameter	m
$\vec{h}$	Vertical distance from particle center to pore center	m
J_v	Vapor flux	$\mathrm{kg\,m^{-2}\,s^{-1}}$
L	Latent heat of fusion	$\mathrm{J\,kg^{-1}}$
K	Thermal conductivity of air	$\mathrm{J\,m^{-1}\,s^{-1}\,K^{-1}}$
m	Particle mass	kg
P	Probability	–
p_s	Equilibrium vapor pressure at particle surface	Pa
p_eq	Equilibrium vapor pressure over planar surface	Pa
p_{amb}	Ambient (environmental) vapor pressure	Pa
$\mathrm{R_v}$	Specific gas constant for vapor	$\mathrm{J\,kg^{-1}\,K^{-1}}$
r	Particle radius	m
$\bar{r}$	Mean particle radius	m
r_e	Effective radius	m
r_e0	Initial effective radius	m
r_n	Number-median radius	m
$\hat{S}$	Specific surface area	$\mathrm{m^2\,kg^{-1}}$
$\hat{S}_0$	Initial specific surface area	$\mathrm{m^2\,kg^{-1}}$
T	Temperature	K
z	Distance along temperature gradient axis	m
γ	Surface tension of ice against air	$\mathrm{J\,m^{-2}}$
κ	Empirical parameter for SSA evolution	–
ρ_i	Density of ice	$\mathrm{kg\,m^{-3}}$
ρ_s	Density of snow	$\mathrm{kg\,m^{-3}}$
ρ_v	Density of water vapor	$\mathrm{kg\,m^{-3}}$
$\rho_\mathrm{v,s}$	Equilibrium vapor density at particle surface	$\mathrm{kg\,m^{-3}}$
$\rho_\mathrm{v,amb}$	Ambient (environmental) vapor density	$\mathrm{kg\,m^{-3}}$
σ_g	Geometric standard deviation	–
τ	Empirical parameter for SSA evolution	hr
ϕ	Model parameter, interparticle spacing irregularity	–

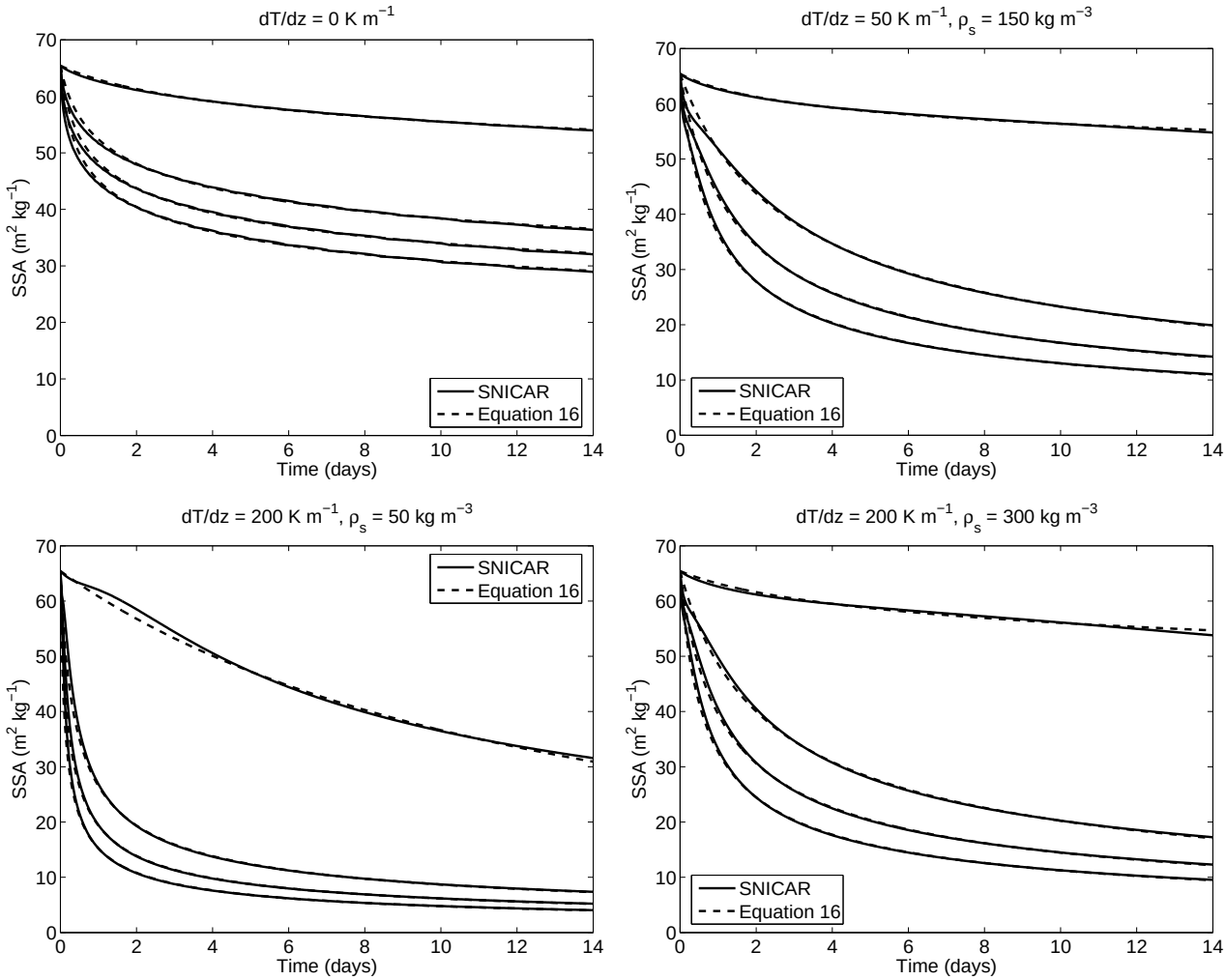

Figure 5. Comparison of modeled specific surface area (SSA) evolution with parameterization from Equation 16, using best-fit parameters for τ and κ. Each plot depicts SSA evolution for a given TG and ρ_s with snow temperatures of (curves from top to bottom) -50, -20, -10, and 0 °C.

frost formation are also needed for a thorough understanding of snow albedo evolution. This study also highlights the need for high-resolution experimental studies that simultaneously observe snow temperature gradient, SSA, accumulation of soot and dust, and albedo. Such data would provide stronger basis for defining model parameters describing snow SSA and albedo evolution. If models are to accurately predict climate changes due to greenhouse and other forcings, they must capture influences of all important processes involved in snowpack evolution.

Appendix A: List of Symbols

(See Table 5 at end)

Acknowledgments. We thank three anonymous reviewers for critical analysis and helpful comments about our methods. We thank Teruo Aoki for providing snow grain size measurements, Anne-Sophie Taillandier and Florent Domine for providing advice and references about SSA evolution, Michael Lehning and Charles Fierz for providing snow grain size observations, Jeff Dozier and Walter Rosenthal for comments on sintering, and Steve Warren for advice on relationships between size distributions and albedo. Data were obtained from the NSF supported Niwot Ridge Long-Term Ecological Research project and the University of Colorado Mountain Research Station. Funding for this work was provided by NSF/NCAR SGER ATM-0503148 and NASA Earth System Science Fellowship NNG05GP30H. Computations supported by Earth System Modeling Facility NSF ATM-0321380.

References

Adams, E. E., and R. L. Brown (1982), A model for crystal development in dry snow, *Geophys. Res. Lett.*, *9*(11), 1287–1289.

Adams, E. E., and R. L. Brown (1983), Metamorphism of dry snow as a result of temperature gradient and vapor density differences, *Ann. Glaciol.*, *4*, 1–9.

Akitaya, E. (1974), Studies on depth hoar, *Contrib. Inst. Low Temp. Sci., Ser. A*, *26*(67).

Aoki, T., T. Aoki, M. Fukabori, A. Hachikubo, Y. Tachibana, and F. Nishio (2000), Effects of snow physical parameters on spectral albedo and bidirectional reflectance of snow surface, *J. Geophys. Res.*, *105*(D8), 10,219–10,236.

Aoki, T., A. Hachikubo, and M. Hori (2003), Effects of snow physical parameters on shortwave broadband albedos, *J. Geophys. Res.*, *108*(D19), doi:10.1029/2003JD003506.

Arons, E. M., and S. Colbeck (1995), Geometry of heat and mass transfer in dry snow: A review of theory and experiment, *Rev. Geophys.*, *33*(4), 463–493.

Baunach, T., C. Fierz, P. K. Satyawali, and M. Schneebeli (2001), A model for kinetic grain growth, *Ann. Glaciol.*, *32*, 1–6.

Brown, R. L., P. K. Satyawali, M. Lehning, and P. Bartelt (2001), Modeling the changes in microstructure of snow during metamorphism, *Cold Reg. Sci. Tech.*, *33*, 91–101.

Brun, E. (1989), Investigation of wet-snow metamorphism in respect of liquid-water content, *Ann. Glaciol.*, *13*, 22–26.

Bryant, F. D., and P. Latimer (1969), Optical efficiencies of large particles of arbitrary shape and orientation, *J. Colloid Interface Sci.*, *30*, 291–304.

Budyko, M. I. (1969), The effects of solar radiation on the climate of the earth, *Tellus*, *21*, 611–619.

Cabanes, A., L. Legagneux, and F. Domine (2003), Rate of evolution of the specific surface area of surface snow layers, *Environ. Sci. Tech.*, *37*(4), 661–666.

Chiruta, M., and P. K. Wang (2003), The capacitance of rosette ice crystals, *J. Atmos. Sci.*, *60*, 836–846.

Colbeck, S. C. (1980), Thermodynamics of snow metamorphism due to variations in curvature, *J. Glaciol.*, *26*(94), 291–301.

Colbeck, S. C. (1983a), Theory of metamorphism of dry snow, *J. Geophys. Res.*, *88*(C9), 5475–5482.

Colbeck, S. C. (1983b), Ice crystal morphology and growth rates at low supersaturations and high temperatures, *J. Appl. Phys.*, *54*(5), 2677–2682.

Colbeck, S. C. (1993), The vapor diffusion coefficient for snow, *Water Resour. Res.*, *29*(1), 109–115.

Colbeck, S. C. (2001), Sintering of unequal grains, *J. Appl. Phys.*, *89*(8), 4612–4618.

Domine, F., and P. B. Shepson (2002), Air-snow interactions and atmospheric chemistry, *Science*, *297*, 1506–1510.

Douville, H., J.-F. Royer, and J.-F. Mahfouf (1995), A new snow parameterization for the Meteo-France climate model Part I: validation in standalone experiments, *Climate Dyn.*, *12*, 21–35.

Dozier, J. (1989), Spectral signature of alpine snow cover from the Landsat Thematic Mapper, *Remote Sens. Environ.*, *28*, 9–22.

Fierz, C., and T. Baunach (2000), Quantifying grain shape changes in snow subject to large temperature gradients, *Ann. Glaciol.*, *31*, 439–444.

Flanner, M. G., and C. S. Zender (2005), Snowpack radiative heating: Influence on Tibetan Plateau climate, *Geophys. Res. Lett.*, *32*, L06501, doi:10.1029/2004GL022076.

Fukuzawa, T., and E. Akitaya (1993), Depth-hoar crystal growth in the surface layer under high temperature gradient, *Ann. Glaciol.*, *18*, 39–45.

Giddings, J. C., and E. LaChapelle (1962), The formation rate of depth hoar, *J. Geophys. Res.*, *67*(6), 2377–2383.

Grenfell, T., S. Warren, and P. Mullen (1994), Reflection of solar radiation by the Antarctic snow surface at ultraviolet, visible, and near-infrared wavelengths, *J. Geophys. Res.*, *99*(D9), 18,669–18,684.

Grenfell, T. C., and S. G. Warren (1999), Representation of a nonspherical ice particle by a collection of independent spheres for scattering and absorption of radiation, *J. Geophys. Res.*, *104*(D24), 37,697–31,709.

Grenfell, T. C., S. P. Neshyba, and S. G. Warren (2005), Representation of a nonspherical ice particle by a collection of independent spheres for scattering and absorption of radiation: 3. Hollow columns and plates, *J. Geophys. Res.*, *110*, D17203, doi:10.1029/2005JD005811.

Gubler, H. (1985), Model for dry snow metamorphism by interparticle vapor flux, *J. Geophys. Res.*, *90*(D5), 8081–8092.

Hansen, J., and L. Nazarenko (2004), Soot climate forcing via snow and ice albedos, *PNAS*, *101*(2), 423–428.

Hood, E., M. Williams, and D. Cline (1999), Sublimation from a seasonal snowpack at a continental, mid-latitude alpine site, *Hydrol. Process.*, *13*, 1781–1797.

Jordan, R. (1991), A one-dimensional temperature model for a snow cover: Technical documentation for SNTHERM 89., *Tech. Rep. Special Report 91-16*, U.S. Army Cold Regions Research and Engineering Laboratory.

Kamata, Y., S. A. Sokratov, and A. Sato (1999), Temperature and temperature gradient dependence of snow recrystallization in depth hoar snow, *Lecture Notes in Physics*, *533*, 395–402.

Legagneux, L., A.-S. Taillandier, and F. Domine (2004), Grain growth theories and the isothermal evolution of the specific surface area of snow, *J. Appl. Phys.*, *95*(11), 6175–6184.

Lehning, M., P. Bartelt, B. Brown, C. Fierz, and P. Satyawali (2002), A physical SNOWPACK model for the Swiss avalanche warning Part II. Snow microstructure, *Cold. Reg. Sci. Tech.*, *35*, 147–167.

Loth, B., and H.-F. Graf (1998), Modeling the snow cover in climate studies 1. Long-term integrations under different climatic conditions using a multilayered snow-cover model, *J. Geophys. Res.*, *103*(D10), 11,313–11,327.

Marbouty, D. (1980), An experimental study of the temperature-gradient metamorphism, *J. Glaciol.*, *26*(94), 303–312.

Marshall, S., and R. Oglesby (1994), An improved snow hydrology for GCMs. Part 1: Snow cover fraction, albedo, grain size, and age, *Climate Dyn.*, *10*, 21–37.

Marshall, S. E. (1989), A physical parameterization of snow albedo for use in climate models, Ph.D. thesis, The University of Colorado at Boulder, Boulder, CO.

McGuffie, K., and A. Henderson-Sellers (1985), The diurnal hysteresis of snow albedo, *J. Glaciol.*, *31*, 188–189.

Miller, D. A. (2002), An integrated microstructural study of dry snow metamorphism under generalized thermal conditions, Ph.D. thesis, Montana State University, Bozeman, MT.

Miller, D. A., E. E. Adams, and R. L. Brown (2003), A microstructure approach to predict dry snow metamorphism in generalized thermal conditions, *Cold Reg. Sci. Tech.*, *37*, 213–226.

Neshyba, S., T. Grenfell, and S. Warren (2003), Representation of a nonspherical ice particle by a collection of independent spheres for scattering and absorption of radiation: 2. hexagonal columns and plates, *J. Geophys. Res.*, *108*(D15), 10.1029/2002JD003,302.

Oleson, K. W., et al. (2004), Technical description of the Community Land Model (CLM), *Tech. Rep. NCAR/TN–461+STR*, National Center for Atmospheric Research.

Painter, T. H., and J. Dozier (2004), Measurements of the hemispherical-directional reflectance of snow at fine spectral and angular resolution, *J. Geophys. Res.*, *109*, D18115, doi:10.1029/2003JD004458.

Pirazzini, R. (2004), Surface albedo measurements over Antarctic sites in summer, *J. Geophys. Res.*, *109*, D20118, doi:10.1029/2004JD004617.

Pollack, J. B., and J. N. Cuzzi (1980), Scattering by nonspherical particles of size comparable to a wavelength: A new semi-empirical theory and its application to tropospheric aerosols, *J. Atmos. Sci.*, *37*, 868–881.

Pruppacher, H. R., and J. D. Klett (1998), *Microphysics of Clouds and Precipitation*, second ed., 954 pp., Kluwer Acad. Publ., Dordrecht, Holland.

Rogers, R. R., and M. K. Yau (1994), *A Short Course in Cloud Physics*, third ed., Pergamon Press, Oxford, UK.

Rosenthal, W., and J. Saleta (2006), Scanning electron miscroscopy of impurity structures in snow, *Cold. Reg. Sci. Tech.*, *in press*.

Schmidt, G. A., et al. (2006), Present day atmospheric simulations using GISS ModelE: Comparison to in-situ, satellite and reanalysis data, *J. Climate*, *in press*.

Schneebeli, M., and S. A. Sokratov (2004), Tomography of temperature gradient metamorphism of snow and associated changes in heat conductivity, *Hydrol. Process.*, *18*, 3655–3665, doi:10.1002/hyp.5800.

Seinfeld, J. H., and S. N. Pandis (1998), *Atmospheric Chemistry and Physics*, 1326 pp., John Wiley & Sons, New York, NY.

Sokratov, S. A. (2001), Parameters influencing the recrystallization rate of snow, *Cold. Reg. Sci. Tech.*, *33*(2–3), 263–274.

Sommerfeld, R. A. (1983), A branch grain theory of temperature gradient metamorphism in snow, *J. Geophys. Res.*, *88*(C2), 1484–1494.

Stephenson, P. J. (1967), Some considerations of snow metamorphism in Antarctic ice sheet in the light of ice crystal studies, in *Physics of Snow and Ice, Part II*, Institute for Low Temperature Science, Hokkaido University.

Sturm, M., and C. S. Benson (1997), Vapor transport, grain growth and depth-hoar development in the subarctic snow, *J. Glaciol.*, *43*(143), 42–59.

Toon, O. B., C. P. McKay, T. P. Ackerman, and K. Santhanam (1989), Rapid calculation of radiative heating rates and photodissociation rates in inhomogeneous multiple scattering atmospheres, *J. Geophys. Res.*, *94*(D13), 16,287–16,301.

Verseghy, D. L. (1991), CLASS–A Canadian land surface scheme for GCMs. I. Soil model, *Int. J. Climatology*, *11*, 111–133.

Warren, S., and W. Wiscombe (1980), A model for the spectral albedo of snow. II: Snow containing atmospheric aerosols, *J. Atmos. Sci.*, *37*, 2734–2745.

Warren, S. G., T. C. Grenfell, and P. C. Mullen (1986), Optical properties of Antarctic snow, *Antarctic Journal of the Unites States*, *21*(5).

Williams, M. A. (2005), Niwot Ridge Subnivean Data Retrieval System, Niwot Ridge Long Term Ecological Research Project, `http://culter.colorado.edu`.

Wiscombe, W. J., and S. G. Warren (1980), A model for the spectral albedo of snow. I: Pure snow, *J. Atmos. Sci.*, *37*, 2712–2733.

Yang, F., A. Kumar, W. Wang, H.-M. H. Juang, and M. Kanamitsu (2001), Snow-albedo feedback and seasonal climate variability over North America, *J. Climate*, *14*, 4245–4248.

Zhang, W., and J. H. Scneibel (1995), The sintering of two particles by surface diffusion and grain boundary diffusion – a two-dimensional numerical study, *Acta Metall. Mater.*, *43*(12), 4377–4386.

M. G. Flanner and C. S. Zender, Department of Earth System Science, University of California, Irvine, CA 92697-3100. (mflanner@uci.edu)